WO_{3-x} Nanorods Synthesized on a Thermal Hot Plate

Fook Chiong Cheong,[†] Binni Varghese,[†,‡] Yanwu Zhu,[†,‡] Eunice Phay Shing Tan,[§] Ling Dai,[‡,§] Vincent B. C. Tan,[‡,§] Chwee Teck Lim,[‡,§] and Chorng Haur Sow*[,†,‡]

Department of Physics, BLK S12, Faculty of Science, National University of Singapore, 2 Science Drive 3, Singapore 117542, Department of Mechanical Engineering, National University of Singapore, 9 Engineering Drive 1, Singapore 117576, and National University of Singapore Nanoscience and Nanotechnology Initiative, 2 Science Drive 3, Singapore 117542

Received: June 13, 2007; In Final Form: September 12, 2007

A simple thermal vapor deposition technique to synthesize crystalline tungsten oxide nanorods in ambient condition is presented. Using a commercial thermal hot plate, a pure 99.9% tungsten foil is heated at 485 ± 5 °C under ambient conditions with a piece of 150 μm thick glass cover slide pressing on the tungsten foil. Single crystalline WO_{3-x} nanorods, with a preferential growth axis in the [001] direction, are found to deposit on the cover slide facing the heated tungsten foil. The structure, morphology, and composition of the WO_{3-x} nanorods were characterized using the scanning electron microscopy, transmission electron microscopy, energy dispersive spectrometry, Raman spectroscopy, and X-ray diffraction. In addition, mechanical properties of the as-synthesized nanorods were investigated by employing the three-point bend test using an atomic force microscope. The elastic modulus of the nanorods was found to be in the 10−110 GPa range, and it increases with decreasing diameter of the nanorods. The tungsten oxide nanorod was also found to be a good field emitter with a field enhancement factor estimated to be 9.8×10^4 cm^{-1}.

1. Introduction

One-dimensional metal oxide nanostructures have been studied extensively due to their unique chemical and physical properties.[1−9] Among these nanostructured metal oxides, the tungsten oxide nanostructure offers a wide spectrum of potential applications in devices such as electrochromic devices,[1,2] chemical sensors,[3] and electrocatalyst.[7] WO_{3-x} nanowires were found to be good materials for electrochromic devices[1] because they have short bleach coloration transition time.[2] A large surface to volume ratio of one-dimensional tungsten oxide nanomaterials, like bundles of $W_{18}O_{49}$ nanowires, gives rise to extraordinary high sensitivity at a low concentration of NO_2.[3] Furthermore, WO_x thin film has also been demonstrated to be a promising catalyst for electrochemical oxidation of organic compounds.[7] In addition, the high aspect ratio of tungsten nanotips makes them ideal candidates for field emitters with a relatively low threshold turn-on field.[9]

A few approaches have been reported on the synthesis of tungsten oxide nanostructures. These methods include the wet chemistry approach,[10,11] irradiation method,[12−14] chemical vapor deposition,[15] and high-temperature physical vapor deposition.[16−20] For example, Gu et al. utilized the self-assembly of wet chemically precipitated h-WO_3 to obtain ordered crystalline nanostructures.[10] Xiao et al. synthesized porous polycrystalline $W_{18}O_{49}$ nanowires with repeated filling of a tungsten oxide based colloidal solution in porous anodic alumina followed by thermal heating at 650 °C.[11] Researchers have also developed a laser irradiation thermal deposition method to synthesize WO_x nanostructures. For example, Li et al.[13,14] made use of an infrared laser irradiation to heat up W foil or filament to a temperature above 1000 °C to produce $W_{18}O_{49}$ and WO_3. WO_3 nanowires can also be synthesized successfully via chemical vapor deposition at an elevated temperature of 900 °C.[15] Using a thermal approach, other methods for synthesizing WO_x nanostructures have also been reported. For example, Zhuo et al. reported the use of high temperature of 1400 °C to physically vaporize tungsten and deposit the resultant WO_x onto a Si(111) surface.[16] Gu et al. had also obtained tungsten oxide nanowires by heating tungsten metal plates at 700 °C in argon atmosphere.[17] By coating metallic tungsten plate with potassium halide salt, doped tungsten oxide nanowires were also found to grow on the tungsten plate at a heating temperature of 625 °C.[18] High-purity WO_3 can also be produced by passing a 1.2 A current across a tungsten filament under 10^{-4} Torr for 48 h with the apex of the wire heated up to approximate 1400 °C.[19] Wrapped with boron oxide vitreous powder at 1600 °C on tungsten wire, WO_2 nanowires were also produced by the thermal deposition method.[20] Furthermore, $W_{18}O_{49}$ whiskers can be prepared by oxidizing a tungsten thin film with H_2O and subsequently annealing it at a temperature of over 900 °C under a pressure of about 1 Torr.[21] In addition, large-scale WO_3 can be prepared by a hydrothermal approach using citric acid as structure modifier and hexadecylamine as a templating agent.[22] Using controlled removal of surfactant from presynthesized mesolamellar precursor at a temperature of 720 °C at 10^{-2} atm pressure, Li et al. obtained large-scale monoclinic $W_{18}O_{49}$ nanowires.[23]

As new approaches for the synthesis of nanostructured tungsten oxide are continuously being developed, it is also important to develop a new method with desirable practical attributes such as simplicity, mass production, catalyst-free, low-

* Corresponding author. Tel.: 65-65162957. Fax: 65-67776126. E-mail: physowch@nus.edu.sg.
[†] Department of Physics, National University of Singapore.
[‡] National University of Singapore Nanoscience and Nanotechnology Initiative.
[§] Department of Mechanical Engineering, National University of Singapore.

10.1021/jp074569z CCC: $37.00
Published on Web 10/26/2007

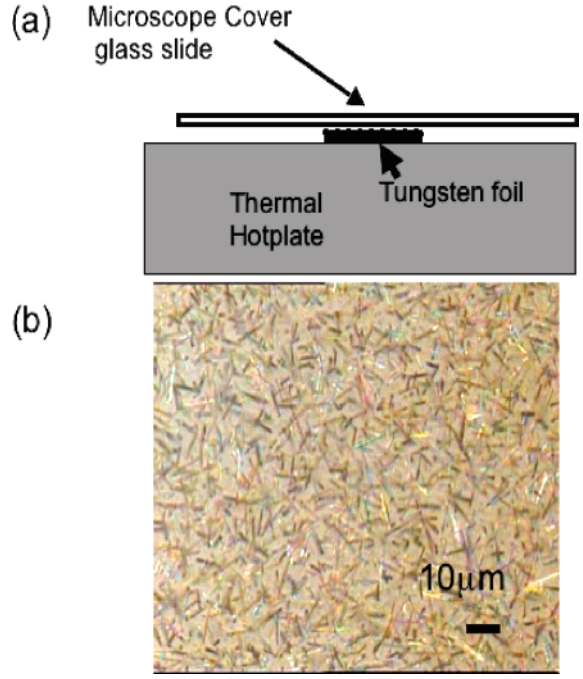

Figure 1. (a) Schematic of the setup used in WO_{3-x} synthesis with the thermal hot plate technique. (b) Optical micrograph of WO_{3-x} nanorods found on the glass cover slides

formation temperature, reasonably low costs, and not requiring extreme pressure conditions. Remarkably, simple heating of metallic film/foil/plate on a thermal hot plate in ambience can give rise to a wide variety of nanostructured metallic oxide with good crystalline order and well-controlled morphologies.[24−27] Continuing our efforts in the synthesis of metal oxide nanostructures,[24−27] here we report a technique to synthesize crystalline tungsten oxide nanorods using this simple and yet surprisingly versatile hot plate technique.

2. Experimental Section

A schematic of the experimental setup for the synthesis of tungsten oxide nanorods is illustrated in Figure 1a. A tungsten foil, together with a cover glass resting on top, was heated on a hot plate in ambient condition. After long duration of heating, nanorods were found deposited on the cover glass placed close to the heated metal foil. This is evident from the optical micrograph of the surface of the cover glass as shown in Figure 1b.

A wide variety of characterization techniques were employed to ascertain the chemical nature, crystalline order, and mechanical properties of these nanorods. These techniques include scanning electron microscopy (SEM, JEOL JSM-6400F), transmission electron microscopy (TEM, JEOL JEM 3010 with inbuild energy dispersive X-ray spectroscopy (EDX)), micro-Raman spectroscopy (Renishaw System2000), photospectroscopy (Shimadzu UV-3600 spectrophotometer), and X-ray diffraction (XRD, Phillips PW 127). These nanorods were found to be crystalline tungsten oxide nanorods with a diameter in the range of about 40−200 nm with a typical length over 15 μm. Characterization of the mechanical properties of the WO_{3-x} nanorods was carried out using an atomic force microscopy (AFM) system (Nanoscope IIIa, Digital Instruments).

To synthesize WO_{3-x} nanostructures, we heated a polished and cleaned 99.9% pure tungsten foil (0.05 mm thick, typical dimension of 10 × 10 mm^2) (Aldrich Chemical Co.) on a Cimarec digital thermal hot plate at about 485 ± 5 °C. The main difference in this work as compared to our earlier reports[24−27] is the placement of a piece of Fisher Scientific microscopic cover glass (35 × 50 mm^2 × 150 μm) on top of the tungsten foil. The samples were heated at different durations (several hours to several days) under ambient condition. After the completion of the heating process, the sample was allowed to cool down to room temperature before removal from the hot plate. Large densities of nanorods were usually found deposited on the cover glass slide surface facing the tungsten foil as shown in Figure 2a.

The nanorods are found deposited directly as a thin film on the transparent cover glass slide. The SEM images, optical spectrum, and X-ray diffraction spectrum of the nanorod thin film were obtained from the nanorods' thin film deposited on the microscope cover glass slide. As for the other studies, the cover glass with the nanorods was first sonicated in distilled water for 10 min to obtain an aqueous suspension of the nanorods. This was then followed by subjecting this aqueous suspension of nanorods to centrifugation to separate and remove tiny particles from the nanorods. A drop of the pure aqueous suspension of nanorods was subsequently dropped onto a TEM grid (Agar Scientific (S166-4) Lacey Carbon 400 Mesh Cu-grid) and left to dry for subsequent imaging purposes. In addition, the same process was carried out onto a DuraSiN (DTM-25232) SiN mesh support substrate with an array of pits with pitch of 10 μm and depth of 200 nm. The nanorods that bridged across the pits were utilized for the Raman spectroscopy study of single nanorods.

For the investigation of mechanical properties, suspended nanorod configuration was archived by drying a drop of nanorod suspension in water on a Si substrate with square holes. The mechanical characterization of the WO_{3-x} nanorods was carried out using the three-point-bend test.[28−33] In this experiment, an AFM tip was used to load and unload the suspended nanorods across square pits, and the resulting deflection was measured from a force curve. By using simple elastic beam bending theory, the elastic Young's modulus of the nanorods was extracted.

To investigate the potential application of WO_{3-x} nanorods as field emitter, an individual nanorod was mounted on the tip of a chemically etched tungsten tip. In order to pick up one nanorod from the as-grown sample on the glass slide, the tungsten tip was adhered with some carbon paste, which was used to stick nanorods selectively with the assistance of a micro-probe station system.

3. Results and Discussion

After heating the cover glass with W foil at 485 ± 5 °C for more than 15 h, a white patch with the same size as the tungsten foil was observed on the cover glass surface facing the foil as shown in Figure 2a. When observed under the optical microscope, nanorods were found dispersed randomly on the surface of the cover glass, as shown in Figure 1b. As for the heated metal foil, we observed that the surface of the heated tungsten foil formed a thin yellowish film of WO_3, but we do not observe any nanorods growing directly on the surface of the metal substrate. This observation is very different compared to the earlier reports of using a hot plate to synthesize metal oxide nanostructures[25,26] in ambience, where the nanostructures are usually found growing on the metal substrate. This suggests that the growth mechanism of the tungsten oxide nanorods in this work is different compared to our previous works on hot plate synthesis of nanomaterials.

Figure 2b shows a large density of nanorods found on the cover glass surface, most of which were micrometers long and

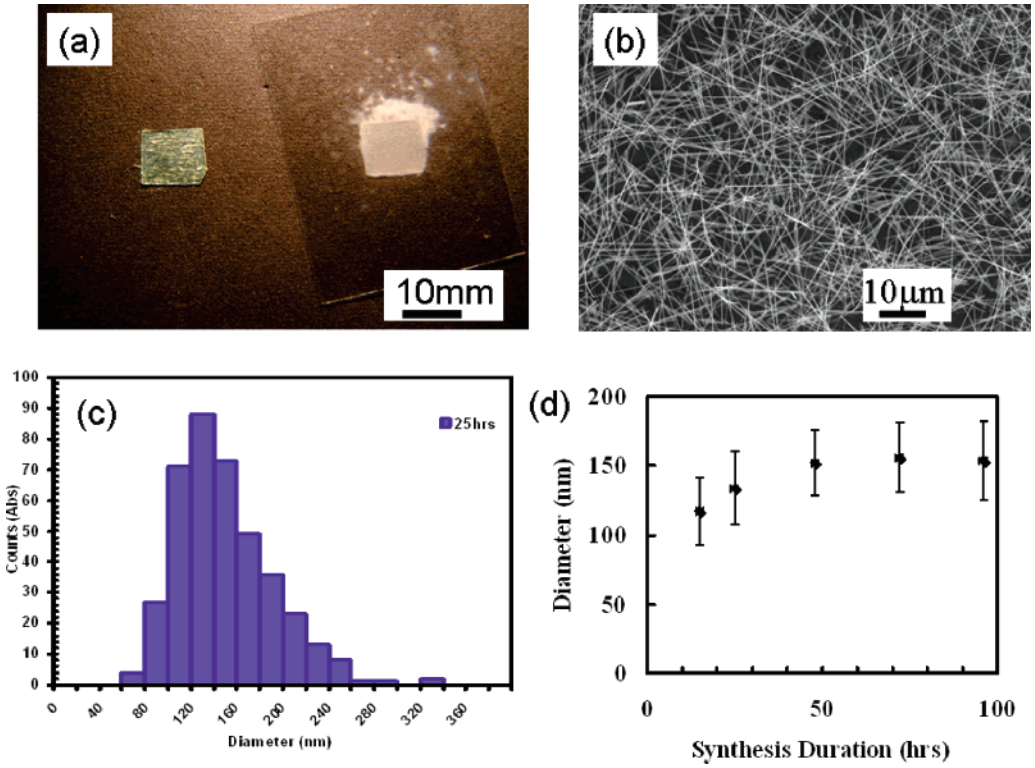

Figure 2. (a) Optical images of the metal foil and the glass slides after heating for 48 h. (b) Electron micrograph of the as-synthesized nanorods on the cover glass. (c) Plot of the nanorods' diameter distribution for the heating duration of 25 h. (d) Plot of average diameter of the nanowires against the growth duration.

with diameters about 130 nm. The density of the nanorods was approximately 7×10^5 nanorods/mm^2 after 25 h of heating. The average diameters of nanorods were found to increase with the duration of heating. After the detail analysis of SEM images, the discrete distribution of the nanorods was obtained. Figure 2c shows the diameter distributions of nanorods formed after 25 h of heating. The average diameter of nanorods increases with the duration of heating, and it approaches a constant value of about 150 ± 23 nm after about 48 h of synthesis as shown in Figure 2d On the other hand, for a sample that was heated for less than 8 h, nanoparticles were found on the cover glass surface instead of nanorods. At a slightly lower heating temperature of 470 ± 5 °C, no nanorod was found on the cover glass too.

Figure 3a shows the EDX analysis of a single nanorod suggesting that the nanorods mainly consist of tungsten and oxygen. The nanorods synthesized by this technique are not doped with any other elements. The Cu peaks are attributed to the copper grid used as a TEM support structure for the nanorods. Using a standard Cu Kα as radiation source, the XRD spectrum (Figure 3b) of the nanostructures on the cover glass had signature peaks corresponding to tetragonal WO_{3-x} [JCPD: 18−1417].[34] The strongest XRD peak of the as-synthesized tungsten oxide nanostructures at 23° can be indexed to the (001) plane with an interplanar distance of approximately 3.8 ± 0.1 Å, and the second most intense peak matches to (200) with an interplanar distance of approximately 2.6 ± 0.1 Å.

A micro-Raman spectrum on a single nanorod is shown in Figure 4a. A single nanorod that was suspended on a hole in the SiN mesh as shown in the inset of Figure 4a was exposed to a 532 nm laser (using the Renishaw System 2000) to obtain the corresponding Raman spectrum. Similar to a report by Li et al.,[23] the bands between 250 and 450 cm^{-1} correspond to the bending of O−W−O bonds, and the modes between 630 and 900 cm^{-1} are ascribed to the stretching of W−O bonds. The

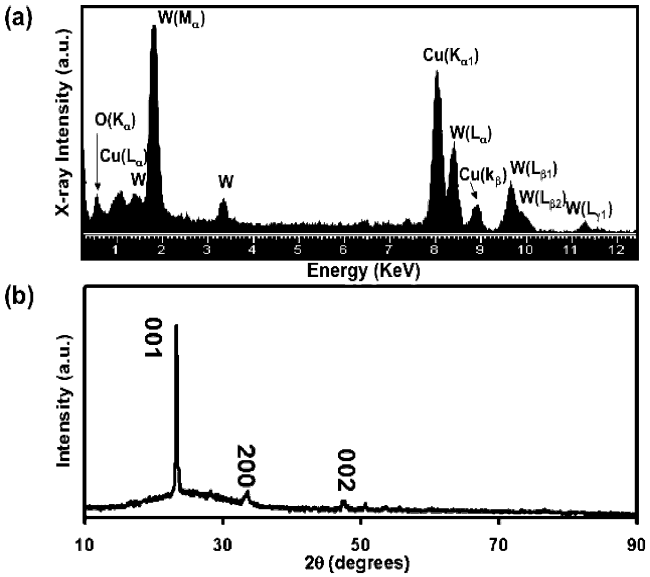

Figure 3. (a) EDX spectrum of one single WO_{3-x} nanorod. (b) XRD signal from the as-synthesized tungsten oxide nanowires on the cover glass substrate.

481 cm^{-1} peak is attributed to the SiN, which was used as the substrate for the deposition of dispersed nanorods.

Since our nanorods are deposited on cover glass slides, it is easy to characterize the optical properties of the sample. Figure 4b shows a typical optical absorption spectrum of the WO_{3-x} nanorod thin film measured at room temperature. The inset shows a plot of the absorption edge, from which the optical band gap, E_g, of the WO_{3-x} film can be derived using $(\alpha h\nu)^2 = A(h\nu - E_g)$, where α is the absorption coefficient, $h\nu$ is the photon energy, A is the edge-width parameter, and E_g is the optical band gap, respectively.[35] Repeated measurements showed that the nanorods had a wide optical band gap of around $4.0 \pm$

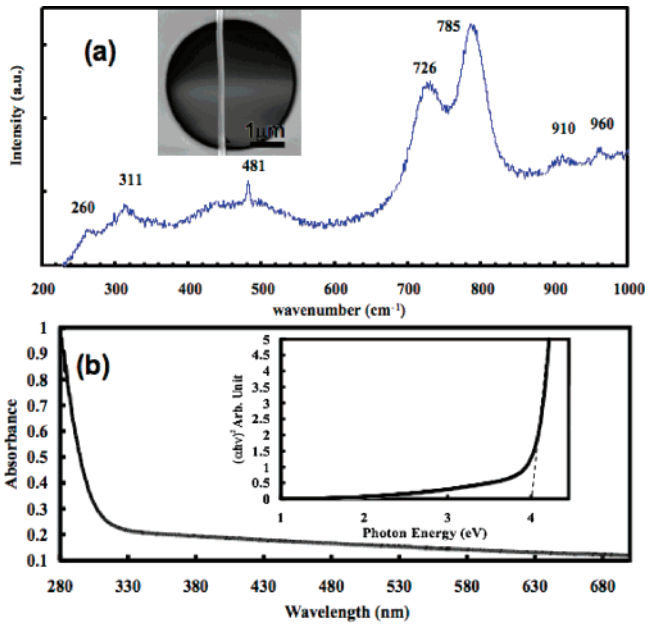

Figure 4. (a) Micro-Raman spectrum of the as-synthesized product deposited on silicon nitrate substrate. Inset is an electron micrograph of the nanorod tested. (b) A typical optical absorption spectrum of the WO_{3-x} nanorods' thin film. Inset is a plot of the absorption edge.

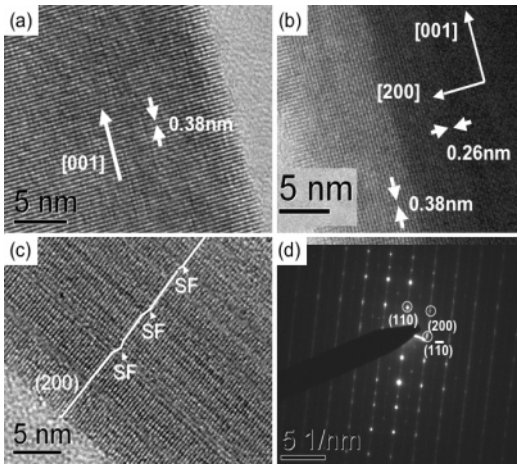

Figure 5. (a) HRTEM micrograph of the WO_{3-x} nanowire. (b) HRTEM of a nanorod showing both the (001) and (200) lattice spacing. (c) TEM micrograph of a segment of the nanorods with a stacking fault in the (200) plane, indicated by arrows marked with 'SF'. (d) ED image of a single nanorod.

0.2 eV. Comparatively, the tungsten oxide nanorods thin film synthesized with this technique have a much wider band gap than previous reported values of polycrystalline and amorphous tungsten oxide thin films, which have band gap values ranging from 2.6 to 3.4 eV.[36] The large range of optical band gap value was attributed to the large distribution of the shape and size of the tungsten oxide nanorods. The variation in the crystallinity of the nanorod could be a contributing factor too.

High-resolution TEM (HRTEM) and electron diffraction (ED) analysis reveal that the nanorods exhibited a single crystalline WO_{3-x} structure. These nanorods exhibited similar structures as reported by Frey et al.[35] for nonstoichiometric tungsten oxide nanostructures. Figure 5 shows a representative HRTEM image of a single tungsten oxide nanorod. The observed preferential growth direction of the nanorods is perpendicular to the (001) plane, as indicated by the white arrow in Figure 5a. Figure 5b shows the neighboring fringe distances were identified as 3.8 $\pm$ 0.1 Å and 2.6 $\pm$ 0.1 Å, corresponding to the (001) and (200) interplanar spacing, respectively. The angle between the two planes is about 90°. The whole nanorod was found to be a single crystal with some stacking faults parallel to the [001] direction as shown in Figure 5c. The formation of stacking faults could be due to the tilting or shifting of the neighboring basal plane caused by thermal stress during the synthesis process. The ED pattern of a nanorod is shown in Figure 5d. From electron diffraction spots, the plane separation of 3.8 Å and 2.6 Å were obtained and were consistent with the interplanar spacing of the (001) and (200) plane, respectively. It is also interesting to note the diffraction spots were smeared into a diffused streak, possibly due to the size effect of the nanowire and/or the presence of stacking faults.[35,37−39] Hence, all the evidence gathered by XRD, ED, and TEM imaging are consistent with tetragonal WO_{3-x} nanorods.

In this report, we propose that solid−vapor−solid is the dominating growth mechanism[14] in our technique. Since we did not introduce any catalyst in the growth process, it is likely that the formation of the nanorods took the route of direct vapor deposition or self-catalytic formation. As this technique was carried out under ambient condition, the tungsten foil surface constantly provided opportunities for tungsten to react with oxygen in the atmosphere to form tungsten oxide. At elevated temperature, the tungsten metal surface was easily oxidized by oxygen in air to form tungsten oxide as evident from the thin yellowish layer of tungsten oxide found on the tungsten foil surface after heating. Although the temperature employed in this hot plate technique is much lower than the melting point of tungsten oxide (>1470 °C),[14] surface melting, evaporation, and oxidization of tungsten can still take place. This tungsten oxide vaporized under a constant heating condition on the thermal hot plate and drifted upward as illustrated in Figure 6b. The vapor would condense onto the lower temperature cover glass surface and nucleate to form nanoparticles at the beginning of growth, as shown in Figure 6b. We noted that there was an issue of oxygen deprivation at the local region between the heated foil and cover glass surface as only a small pocket of air was trapped there. As the tungsten oxide was forming, the oxygen in the small pocket of air was reduced. While a new supply of oxygen from outside may find it hard to efficiently reach this small region, the resultant oxide formed would have a slightly lower oxidation state than that of WO_3. Therefore, the nanorods synthesized are likely to be WO_{3-x}, instead of WO_3. During the condensation (Figure 6c), the vapor aggregated to form the nanorods because the rate of crystal growth is higher in the [001] direction than the piling rate in the [200] direction.[37] Thus, one-dimensional WO_{3-x} nanorods were found on the cover glass when the whole system was cooled down (Figure 6d).

To test our proposed mechanism, time-dependent studies on the growth of the nanorods on the glass surface were investigated. Samples were prepared at increasing durations following the method described earlier, and electron microscopy was utilized to investigate the morphologies of the nanostructures on the cover glasses. At 8 h of heating, the tungsten oxide vapor would condense onto the lower temperature cover glass surface and nucleate to form nanoparticles at the beginning of growth, as shown in Figure 7a. These nanoparticles acted as seed for nucleation of the tungsten oxide vapor. Upon longer heating duration, the deposition would grow thicker as shown in Figure 7b. With extended heating duration of 15 h, long nanorods were observed to grow from some particles on the substrate (Figure 7c). At longer duration of 25 h, high density and high aspect ratio nanorods of WO_{3-x} were obtained (Figure 7d).

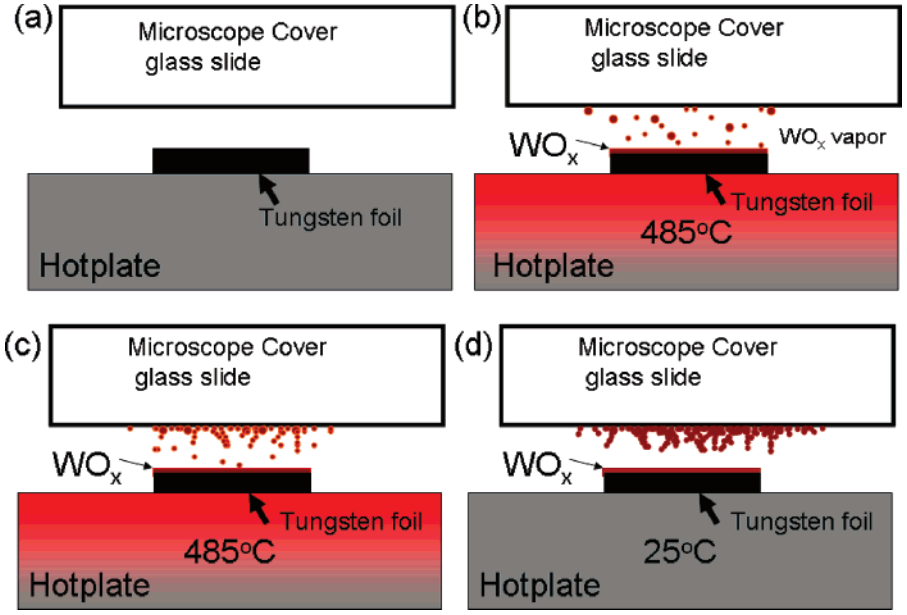

Figure 6. Schematic of the proposed growth mechanism of the nanorods using the hot plate technique. (Diagram not drawn to scale.)

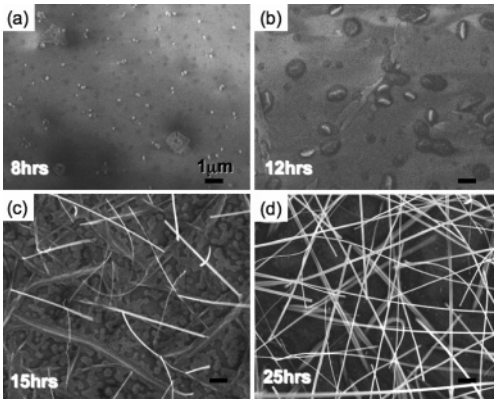

Figure 7. Electron micrograph of nanoparticles of tungsten oxide deposited on the cover glass slide after (a) 8, (b) 12, (c) 15, and (d) 25 h.

For future applications of the nanorods, a fundamental understanding of the mechanical properties is necessary. In this work we report a systematic study on the effect of size on the Young's modulus of the WO_{3-x} nanorods. A drop of the aqueous nanorods suspension was first deposited on a silicon substrate with square holes where many isolated nanorods were found to bridge across these holes as the suspension dried up. On a selected area where a suspended nanorod was found, force curves were obtained using the force volume ($F-V$) mode of the AFM. In this mode, an AFM cantilever will first approach the sample (loading) until a preset cantilever deflection is achieved. The cantilever is then retracted (unloading) to its original position, and a corresponding force curve is obtained. Figure 8a shows a typical $F-V$ image of a suspended nanorod. In our experiment, prior to each $F-V$ image, the area with the suspended nanorod was imaged in contact mode, and the vertical height difference between the silicon surface and the nanorod was used to measure the diameter of the nanorod. The geometrical parameters of the nanorod were measured from a contact-mode AFM image prior to each $F-V$ imaging. During the tests, a cantilever with a spring constant of 0.57 nN/nm was used, and the maximum force exerted by the tip was kept below 40 nN. From the $F-V$ image, the force curve (force−deflection curve) at the midpoint of the suspended nanowire was selected. The deflection (δ) at the midpoint of the suspended nanorod was obtained by subtracting the piezo Z-value on a hard surface (silicon substrate) from the corresponding value of the as-measured force curve at the same applied force as shown in Figure 8b. The nanorod deflection is less than 30 nm as shown in Figure 8c. From the linearity of the force versus deflection curve, it is reasonable to assume that the nanorod underwent elastic bending. Hence, the Young's modulus of the nanorod can be obtained from the three-point bending of a beam with two ends fixed[29] as

$$E = \frac{FL^3}{192\delta I} \tag{1}$$

where F is the maximum force, L is the suspended length of the nanowire, δ is the deflection, and I is the second moment of area of the nanowire, where $I = \pi D^4/64$, with D as the diameter of the nanorod.

Nanorods with diameters ranging from 100 to 300 nm were analyzed to investigate the effect of size on the Young's modulus. Figure 8d shows the measured values of the Young's modulus (E) as a function of the diameter of the nanorods. It is evident that the reduction in the diameters of the nanorods resulted in the increase in the elastic modulus. A possible explanation for this variation in elastic modulus with respect to the nanorod diameter is the possible reduction in the defects within the nanorods as the size is reduced.

To determine the theoretical limit of the elastic modulus, ab initio calculations were performed to determine the Young's modulus of single crystal tungsten oxide, WO_3. The single crystal properties were then used to obtained bounds on the elastic properties of bulk WO_3. Comparisons were made between these bulk values and the experimental results.

In accordance with our experimental observations, the tetragonal WO_3 structure was modeled. Normally WO_3 possesses a defect-free monoclinic structure at room temperature.[40] However, oxygen deprivation leads to WO_{3-x}. This causes a strong lattice relaxation, accompanied by significant transformations in the crystal structure [41,42] possibly as a result of crystallographic shear effect.[43]

We applied CASTEP, a package for the density functional theory (DFT) calculation, to carry out the numerical studies.[44] Plane wave functions were used at a cutoff energy of 400 eV,

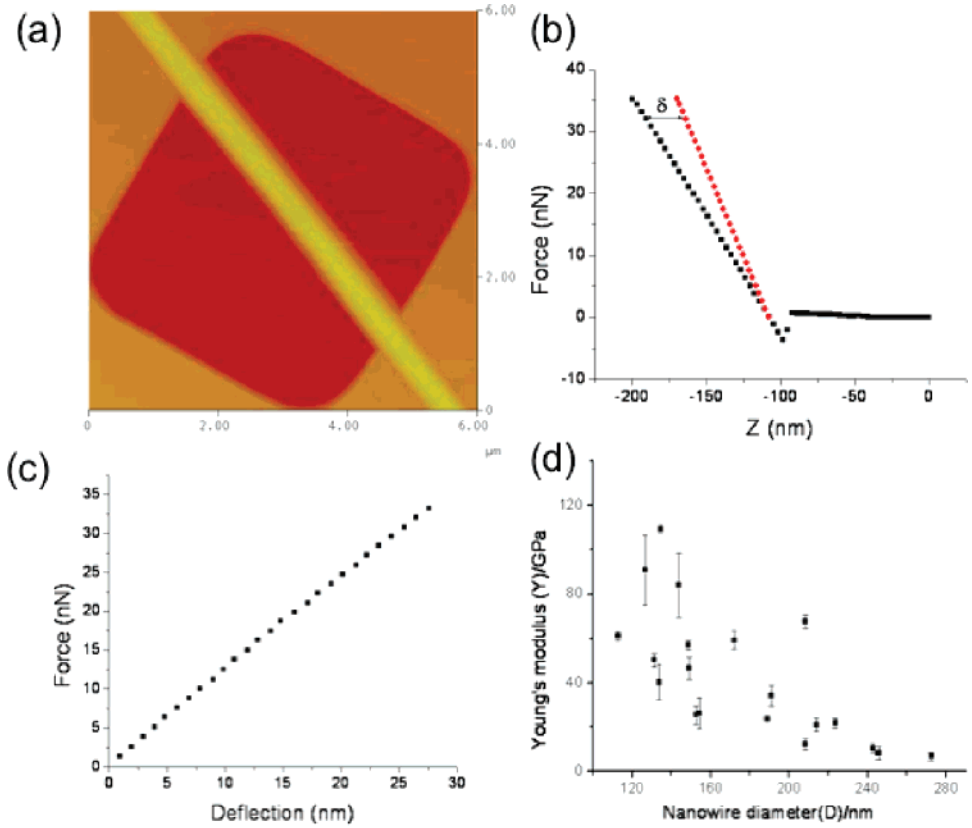

Figure 8. (a) AFM image showing a single WO_{3-x} nanorod lying over the silicon substrate with square pits. (b) Plot of applied force versus *Z*-position of the scanner for reference surface and nanorod. (c) Plot of applied force versus deflection of the nanorod. (d) Plot of the Young's modulus *E* against the nanorod diameter.

TABLE 1: Elastic Constants and Mechanical Properties of Tetragonal WO_3 Structure (GPa)

c_{11}	c_{33}	c_{44}	c_{66}	c_{12}	c_{13}	shear modulus	Young's modulus
387.31	581.06	70.64	277.12	247.66	41.64	122.59 ± 13.82	310.93 ± 14.83

and ultrasoft pseudopotentials and Perdew−Burke−Ernzerhof forms of generalized gradient approximations were selected for the atomic cores and electron exchange-correlation functions.[45] With such settings and parameters, we obtained an equilibrated crystal structure with lattice parameters $a = 5.412$ Å, $c = 3.826$ Å. These are in good agreement with the experimental results of tetragonal WO_3.

With the optimized structures, the elastic constants, c_{ij}, with respect to various strain conditions, were calculated as the second derivatives of the energy density

$$C_{ij} = \frac{1}{V}\left(\frac{\partial^2 U}{\partial \epsilon_i \partial \epsilon_j}\right) \quad (2)$$

where V is the structural volume, U is the total energy, and ϵ_{ij} is the strain in directions i and j. For a homogeneous tetragonal structure, six independent elastic constants—c_{11}, c_{33}, c_{44}, c_{66}, c_{12}, and c_{13}—contribute to the bulk properties. The theory of Hashin−Shtrikman (HS) was employed to obtain the mechanical properties of the bulk tetragonal WO_3 structure as shown in Table.1.[46]

The Young's modulus from the theoretical computation is 310 GPa. This is more than 3 times the value obtained experimentally from the bending tests for the smallest nanorod. The calculated value represents the stiffness of defect-free polycrystalline WO_3, i.e., the upper bound in the absence of defects such as the stacking faults observed in the nanorods. Such defects could greatly reduce the degree of close packing of the material, and thus larger nanorods have lower stiffness as the stacking defaults play more dominant roles. Moreover, the reduction of oxygen could also give rise to defects such as vacancies inside the crystals, which further reduce material stiffness.

One-dimensional nanostructures are usually good candidates for field emitters. In this work, we have also studied field emission from a single nanorod. Figure 9a shows a SEM image of a WO_{3-x} nanorod on a tungsten tip. The nanorod has a length of about 20 μm and a diameter of about 140 nm. The measurements of FE properties of the nanorod was carried out using two-points configuration in a vacuum chamber with a pressure of about 1.5×10^{-6} Torr. The nanorod was adhered to a tungsten tip with some carbon paste as cathode as shown in Figure 9a. The anode is another similar tungsten tip, which has the axis of the tip aligned with the axis of the nanorod. Figure 9b shows the field emission $I-V$ curve of the nanorod with a vacuum distance of about 350 μm. It can be seen that the turn-on voltage is around 640 V and the field emission current reaches a maximum of about 250 nA at a voltage of ~900 V. After 720 V, the field emission curve shows a large fluctuation. Compared with the field emission result from WO_x nanorod films[9] and considering the low vacuum of the field emission chamber, this fluctuation could be attributed to the residual gas adsorption or other environmental vibration or stress under high voltage. The corresponding Fowler−Nordheim (FN) curve ($\ln(I/V^2)$ vs $1/V$) is shown in the inset of Figure 9b, from which a straight line can be fitted with data at high

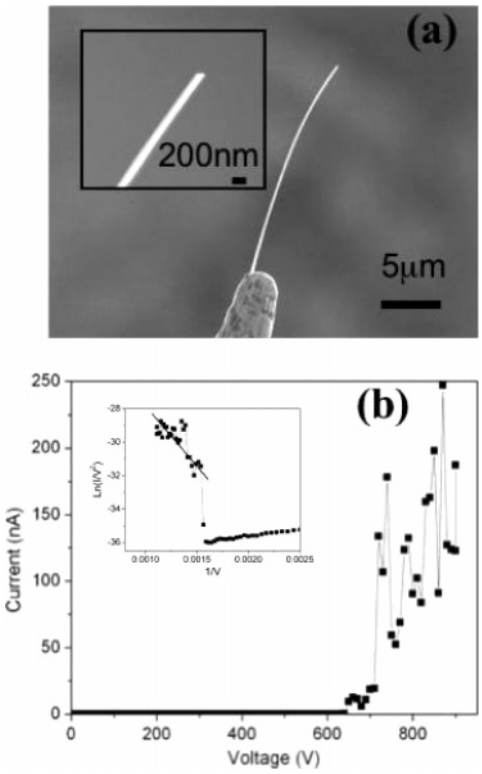

Figure 9. (a) Electron micrograph of a single WO_{3-x} nanorod on a tungsten tip used for single field emission studies. (b) Field emission $I-V$ curve of the nanowire with a vacuum distance of about 350 μm. Inset is the corresponding FN curve.

electric field. This result suggests that the current is from the electron tunneling process.[47] From the FN formula,[48] the enhancement factor can be estimated to be 9.8×10^4 cm^{-1}, which is comparable with the results from single carbon nanotubes[49] and other emitters such as α-Fe_2O_3 nanoflakes on an AFM tip.[48]

4. Conclusion

WO_{3-x} nanorods with relatively large density were synthesized on a large scale on a cover glass using the hot plate technique. The average length and density of the nanorods can be controlled by the duration of synthesis. Electron microscopy and XRD studies support that the nanorods synthesized are tetragonal WO_{3-x} with [001] as the main growth direction. It is also proposed that thermal vapor deposition could be the possible mechanism responsible for the growth of WO_{3-x} nanorods on the cover glass slides. The three-point bend tests on the WO_{3-x} nanorods indicate that the Young's modulus of these nanorods increases as the nanorod diameters decreases. This may be due to reduction in defects in the smaller nanorods. As a plausible application of using these nanorods as field emitters, we investigated a single nanorod's field emitting properties and found it had a field enhancement factor estimated to be 9.8×10^4 cm^{-1}.

References and Notes

(1) Lee, S-H.; Deshpande, R.; Parilla, P. A.; Jones, K. M.; To, B.; Mahan, A. H. and Dillon, A. C. *Adv. Mater*. **2006**, *18*, 763.

(2) Liao, C. C.; Chen, F. R. and J. J. Kai, *Sol. Energy Mater. Sol. Cells*, **2006**, *90*, 1147.

(3) Polleux, J.; Gurlo, A.; Barsan, N.; Weimar, U.; Antonietti, M.; Niederberger, M. *Angew. Chem., Int. Ed.* **2006**, *45*, 261.

(4) Woo, K.; Hong, J.; Ahn, J-P.; Park, J-K.; Kim, K-J. *Inorg. Chem*. **2005**, *44*, 7171.

(5) Ederth, J.; Hoel, A.; Niklasson, G. A.; Granqvist, C. G. *J. Appl. Phys.* **2004**, *96*, 5722.

(6) Ponzoni, A. E.; Comini Sberveglieri, E. G. *Appl. Phys. Lett*. **2006**, *88*, 203101.

(7) Bock, C.; MacDougall, B. *Electrochim. Acta* **2002**, *47*, 3361.

(8) Lee, S. H.; Cheong, H. M.; Tracy, C. E.; et al. *Electrochim. Acta.* **1999**, *44*, 3111.

(9) Zhou, J.; Gong, L.; Shao, Z. D.; et al. *Appl. Phys. Lett.* **2005**, *87*, 223108.

(10) Gu, Z.; Ma, Y.; Yang, W.; Zhange, G.; Yao, J. *Chem. Commun.* **2005**, *28*, 3597.

(11) Xiao, Z.; Zhang, L.; Tian, X.; Fang, X. *Nanotechnology* **2005**, *16*, 2647.

(12) Pfeifer, J.; Badaljan, E. P.; Tekula-Buxbaum, T.; Kovacs, O.; Geszti, A.; Toth, L.; Lunk, H. J. *J. Cryst. Growth* **1996**, *169*, 727.

(13) Li, Y.; Bando, Y.; Golberg, D. *Adv. Mater*. **2003**, *15*, 1294.

(14) Li, Y. B.; Bando, Y.; Golberg, D.; Kurashima, K. *Chem. Phys. Lett.* **2003**, *367*, 214.

(15) Klinke, C.; Hannon, J. B.; Gignac, L.; Reuter, K.; Avouris, P. *J. Phys. Chem. B* **2005**, 17787.

(16) Zhou, J.; Gong, L. Z.; Shao, D.; et al. *Appl. Phys. Lett.* **2005**, *87*, 223108.

(17) Gu, G.; Zheng, B.; Han, W. Q.; Roth, S.; Liu, J. *Nano Lett*. **2002**, *2*, 849.

(18) Hang, Q.; Wang, C.; Liu, J. *Adv. Mater.* **2003**, *15*, 411.

(19) Liu, K.; Foord, D. T.; Scipioni, L. *Nanotechnol.* **2005**, *16*, 10.

(20) Liu, Z.; Bando, Y.; Tang, C. *Chem. Phys. Lett.* **2003**, *372*, 179.

(21) Cho, M. H.; Park, S. A.; Yang, K. D.; et al. *J. Vac. Sci. Technol. B* **2004**, *22*, 1084.

(22) Therese, H. A.; Li, J.; Kolb, U.; Tremel, W. *Solid State Sci*. **2005**, *7*, 67.

(23) Li, X.; Liu, L. J. F.; Li, Y. D. *Inorg. Chem.* **2003**, *42*, 921.

(24) Zhu, Y. W.; Yu, T.; Cheong, F. C.; et al. *Nanotechnology* **2005**, *16*, 88.

(25) Yu, T.; Zhu, Y. W.; Xu, X. J.; et al. *Adv. Mater.* **2005**, *17*, 1595.

(26) Yu, T.; Zhu, Y. W.; Xu, X. J.; et al. *Small* **2006**, *2*, 80.

(27) Zhu, Y. W.; Elim, H. I.; Foo, Y. L.; et al. *Adv. Mater*. **2006**, *18*, 587.

(28) Tan, E. P. S.; Lim, C. T. *Appl. Phys. Lett.* **2004**, *84*, 1603.

(29) Tan, E. P. S.; Goh, C. N.; Sow, C. H.; et al. *Appl. Phys. Lett*. **2005**, *86*, 073115.

(30) Wong, W. E.; Sheehan, P. E.; Lieber, C. M. *Science* **1997**, *277*, 1971.

(31) Salvetat, J. P.; Briggs, A. D.; Bonard, J. M.; Bacsa, R. R.; Kulik, A. J.; Stockli, T.; Burnham, Forrro, N. A. L. *Phys. Rev. Lett.* **1999**, *82*, 944.

(32) Kis, A.; Mihailovic, D.; Remskar, M.; Mrzel, A.; Jesih, A.; Piwonski, I.; Kulik, A. J.; Benoit, W.; Forro, L. *Adv. Mater*. **2003**, *15*, 733.

(33) Silva, E. C. C. M.; Tong, L.; Yip, S.; Vliet, K. J. V. *Small* **2006**, *2*, 239.

(34) Moulzolf, S. C.; LeGore, L. J.; Lad, R. J.; *Thin Solid Films* **2001**, *400*, 56.

(35) Adler, D.; Feinlieb, J. *Phys. Rev. B* **1970**, *2*, 3112.

(36) Frey, G. L.; Rothschild, A.; Sloan, J.; Rosentsveig, R.; Popvitz-Biro, R. P.; Tenne, R. *J. Solid Stat. Chem.*, **2001**, *162*, 300; Sloan, J.; Hutchison, J.; Tenne, R.; Feldman, R. et al, *J. Solid State Chem.* **1999**, *144*, 100.

(37) Paluselli, D.; Marsen, B.; Miller, E. L.; Rocheleau, R. E. *Electrochem. Solid-State Lett.* **2005**, *8*, G301.

(38) Zhao, Y. M.; Li, Y. H.; Ahmad, I.; McCartney, D. G.; Zhu, Y. Q. *Appl. Phys. Lett.* **2006**, *89*, 133116.

(39) Zhou, J.; Ding, Y.; Deng, S. Z.; Gong, L.; Xu, N. S.; Wang, Z. L. *Adv. Mater.* **2005**, *17*, 2110.

(40) Loopstra, B. O.; Boldrini, P. *Acta Crystallogr*. **1966**, *21*, 158.

(41) Karazhanov, S. Zh.; Zhang, Y.; Mascarenhas, A.; Deb, S.; Wang, L. W. *Solid State Ion.* **2003**, *165*, 43.

(42) Sahle, W.; Nygren, M. *J. Solid State Chem*. **1983**, *48*, 154.

(43) Pickering, P.; Tilley, R. J. D. *J. Solid State Chem.* **1976**, *16*, 247.

(44) Clark, S. J.; Segall, M. D.; Pickard, C. J.; Hasnip, P. J.; Probert, M. J.; Refson, K.;Payne, M. C. *Z. Krystallogr*. **2005**, *220*, 567.

(45) Lee, C.; Yang, W.; Parr, R. G. *Phys. Rev. B* **1988**, *37*, 785.

(46) Watt, J. P.; Peseinick, L. *J. Appl. Phys.* **1980**, *51*, 1525.

(47) Fowler, H.; Nordheim, L. W. *Proc. R. Soc. London, Ser. A* **1928**, *119*, 173.

(48) Zhu, Y. W.; Yu, T.; Sow, C. H.; Liu, Y. J.; Wee, A. T. S.; Xu, X. J.; Lim, C. T.; Thong, J. T. L. *Appl. Phys. Lett.* **2005**, *87*, 023103.

(49) Lovall, D.; Buss, M.; Graugnard, E.; Andres, R. P.; Reifenberger, R. *Phys. Rev. B* **2000**, *61*, 5683.